EHD Flow Produced by Electric Corona Discharge (Numerical and Experimental Studies, and Applications)

Lin Zhao and Kazimierz Adamiak

***Abstract*—This paper deals with the numerical simulation, the experimental investigation and the applications of the EHD flow generated by electrical corona discharge in gases. The numerical model based on a hybrid algorithm is presented. The EHD phenomena are investigated with three different electrode configurations and under different working pressures. The transient process of the EHD flow development and the effects of the external gas flow on the EHD flow pattern are discussed. The reliability of the numerical model is verified by the reasonable agreement between the numerical predictions and the experimental measurements. The important roles of the EHD flow in electrostatic precipitators (ESPs) and EHD propulsion unit are discussed.**

***Index Terms*— corona discharge, EHD propulsion, electrohydrodynamics, electrostatic precipitators.**

I. Introduction

THE electrohydrodynamic (EHD) flow is the result of the interaction between drifting ions and the surrounding fluid (gas/liquid) molecules. Both electric field and fluid flow are present and interacting with each other, which makes the analysis of this phenomenon very challenging. This paper presents two numerical models, the decoupled and coupled, to simulate the EHD flow in different situations. Both models are based on a hybrid numerical algorithm based on the Boundary (BEM) and Finite Element (FEM) Methods, the Method of Characteristics (MoC) and the Finite Volume Method (FVM).

The EHD phenomena in three different configurations: the point-plane/mesh, wire-plate, and wire-cylinder are investigated numerically and experimentally to reveal the characteristics of the EHD flow and to verify the proposed model. The EHD dynamics, the effects of external gas flow and the operation pressure on both the corona and the overall flow pattern are also investigated.

Due to the interaction between the electric field and the fluid flow, the presence of the EHD flow increases the complexity of the flow pattern in the precipitation process in industry electrostatic precipitators (ESPs). Meanwhile, because the EHD flow is generated without any mechanical moving parts and the electrical energy is converted directly to the mechanical energy in the process, it finds numerous potential applications, such as in microelectromechanical systems (MEMS), EHD micro-pumps on Mars, the flow pattern modification, heat and mass transfer enhancement, EHD propulsion, etc [1]. The second part of this paper is dedicated to the numerical and experimental studies of the roles of the EHD flow in ESPs and the EHD propulsion unit.

Manuscript received April 17, 2009.

Lin Zhao is with Gannon University, Erie, PA 16541 USA (phone: 814-871-5854; e-mail: zhao001@ Gannon.edu).

Kazimierz Adamiak is with University of Western Ontario, London, ON, N6A5B9, Canada (phone: 519-661-2111 ext: 88358; e-mail: kadamiak@eng.uwo.ca).

II. Mathematical Simulation

A. Numerical Model

A simplified unipolar model of the corona discharge is used in this paper. It is assumed that gas ionization occurs in a very thin layer close to the corona electrode. The thickness of this layer can be neglected. Charged ions of one polarity are injected into the drift zone and all of them move with identical mobility.

The mathematical model of the problem has to include equations for the electric field and space charge density. In the areas with space charge the electric field is governed by the Poisson equation [2]

$$-\varepsilon\nabla^2\Phi = q \tag{1}$$

where Φ is electric potential, q – space charge density and ε – gas permittivity.

The space charge has to satisfy the conservation equation,

$$\nabla \cdot \mathbf{j} = 0 \tag{2}$$

The current density is defined as:

$$\mathbf{j} = q(K_p\mathbf{E} + \mathbf{u}) - D\nabla q \tag{3}$$

where $\boldsymbol{E}$ is the electric field vector, $\boldsymbol{u}$- the gas velocity vector, D - diffusion coefficient, and K_p – the mobility of ions, which changes little with the variation of electric field [3]. In air at atmospheric pressure (760mmHg) and room temperature it can be taken as a constant equal to K_0 =1.8~2.2*10^{-4}m^2/Vs. Under actual pressure it becomes,

$$K_p = \frac{1}{p_{atm}} \times K_0 \tag{4}$$

where p_{atm} is the actual pressure in atm, which is equal to the ratio of the actual pressure to the atmospheric pressure.

Three current density components in (3) are: the drift, convection and diffusion currents. Since the diffusion current

is very small compared to two other components [4], it can be neglected. The drift velocity of ions is usually about two orders of magnitude larger than the typical velocity of the gas flow [5]. Neglecting or keeping the convective component in the ionic current density will lead to two different models of the corona problem: decoupled and fully coupled models.

For a decoupled model, the charge conservation equation becomes [6]:

$$\nabla q \cdot \nabla \Phi = -q^2 / \varepsilon_0 \tag{5}$$

For fully coupled model, the charge conservation equation becomes:

$$\nabla q \cdot (K_p \mathbf{E} + \mathbf{u}) = -K_p q^2 / \varepsilon_0 \tag{6}$$

For either model, two partial differential equations for the electric field have to be solved simultaneously. Formulation of boundary conditions is trivial for Φ, as conducting surfaces are equipotential. The Kaptzov hypothesis is adopted to provide proper boundary conditions for the space charge density, which suggests that the electric field increases proportionally to the corona electrode voltage below the corona onset, but it will preserve its value after the corona is initiated. Peek's formula is used to determine the onset electric field on the corona electrode [6, 7]. In air and at different pressures Peek's formula has the following forms [8]:

$$E_0 = 3.1 \cdot 10^6 \cdot p_{atm}\left(1 + \frac{0.308}{\sqrt{p_{atm} \cdot r_c}}\right) \tag{7}$$

for cylindrical geometry, and

$$E_0 = 3.1 \cdot 10^6 \cdot p_{atm}\left(1 + \frac{0.308}{\sqrt{0.5 \cdot p_{atm} \cdot r_c}}\right) \tag{8}$$

for spherical geometry, where r_c is the electrode radius expressed in cm.

An interaction between space charge and electric field results in a volume Coulomb force, which is responsible for the gas motion. A viscous laminar model for the air flow is assumed, so that the equation of flow continuity and Navier-Stokes equation have to be solved:

$$\nabla \cdot \boldsymbol{u} = 0 \tag{9}$$

$$\rho\left[\frac{\partial \boldsymbol{u}}{\partial t} + (\boldsymbol{u} \cdot \nabla)\boldsymbol{u}\right] = -\nabla P + \eta \nabla^2 \boldsymbol{u} + q \nabla \Phi \tag{10}$$

where: ρ is the gas density, P – static pressure and η – the air viscosity.

The *k-ε* model is adopted to simulate the turbulent flow. In this model, two additional transport equations (for the turbulence kinetic energy, *k*, and the turbulence dissipation rate, *ε*)

$$\frac{\partial}{\partial t}(\rho k) + \frac{\partial}{\partial x_i}(\rho k u_i) = \frac{\partial}{\partial x_j}\left[\left(\mu + \frac{\mu_t}{\sigma_k}\right)\frac{\partial k}{\partial x_j}\right] - \rho\overline{u_i' u_j'}\frac{\partial u_j}{\partial x_i} - \rho\varepsilon + \overline{u_i' f_i'} \tag{11}$$

and

$$\frac{\partial}{\partial t}(\rho\varepsilon) + \frac{\partial}{\partial x_i}(\rho\varepsilon u_i) = \frac{\partial}{\partial x_j}\left[\left(\mu + \frac{\mu_t}{\sigma_\varepsilon}\right)\frac{\partial \varepsilon}{\partial x_j}\right] + C_{1\varepsilon}\frac{\varepsilon}{k}\left(-\rho\overline{u_i' u_j'}\frac{\partial u_j}{\partial x_i}\right) - C_{2\varepsilon}\rho\frac{\varepsilon^2}{k} + \frac{\partial u_i'}{\partial x_i}\frac{\partial f_i'}{\partial x_i} \tag{12}$$

are solved, and the turbulent (or eddy) viscosity μ_t is computed as a function of *k* and *ε* using the following expression

$$\mu_t = \rho C_\mu \frac{k^2}{\varepsilon} \tag{13}$$

where model constants $C_{1\varepsilon}$, $C_{2\varepsilon}$, C_μ, σ_k, and σ_ε have the following default values [9]:

$C_{1\varepsilon} = 1.44$, $C_{2\varepsilon} = 1.92$, $C_\mu = 0.09$, $\sigma_k = 1.0$, $\sigma_\varepsilon = 1.3$.

B. Numerical Algorithm

The numerical algorithm involves two parts: electric field and airflow calculations. The electric field is solved first and the results are then entered into the fluid solver. This part is solved using an algorithm based on hybrid BEM-FEM-MoC techniques. The BEM-FEM method can efficiently handle the electric potential and electric field equations. However, in order to avoid so-called numerical diffusion the MoC was used for predicting the space charge density. The algorithm was arranged into a double iterative loop, converging relatively fast.

Calculated distributions of the electric field and space charge densities were entered into the commercial FLUENT software, where details of the air velocity, pressure and forces can be calculated. For decoupled model, due to one-way coupling (electric field causes gas motion, but motion of air doesn't affect the corona discharge) it is the end of the calculation. For fully coupled model, however, the calculated air velocity is inserted back to the electric field program to update the convective component of the charge conservation equation, and the new cycle of the electric field calculation begins until convergence is reached for all essential electrical and flow parameters [10, 11].

III. Results for Point-Plane/Mesh Geometry

A. Decoupled Mode Verification

The decoupled model has been employed for the simulation of the corona discharge and EHD flow in point-plane/mesh configurations with a corona electrode with the tip radius of curvature of 100 μm, 1 cm above the ground electrode in air at atmospheric pressure [2]. As it was difficult to measure velocity in the air gap, where presence of a probe would distort electric field and airflow, the flow measurement experiment was done in the point-mesh geometry, with the hot wire anemometer probe on the other side of the ground metal mesh. It is reasonable to assume that there is no difference between the metal plane and mesh in terms of the corona simulation (the electric field and the space charge density) if the mesh is sufficiently fine. The experimental apparatuses are shown schematically in Figure 1 (for corona characteristics measurement) and Figure 2 (for air flow measurement).

Experimental and calculated *I-V* characteristics of the discharge agree very well (Figure 3). The difference could be even smaller if the value of the ion mobility, which depends on many different factors like temperature, pressure, humidity and gas composition, would be adjusted. These results also prove that from the electric point of view there is no difference between point-plane and point-mesh geometries.

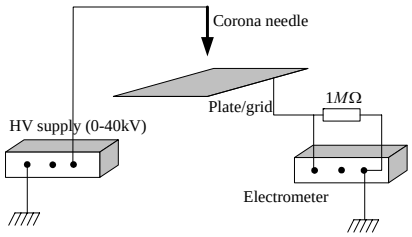

Fig. 1 Schematic view of the experimental set up for I-V curve measurement

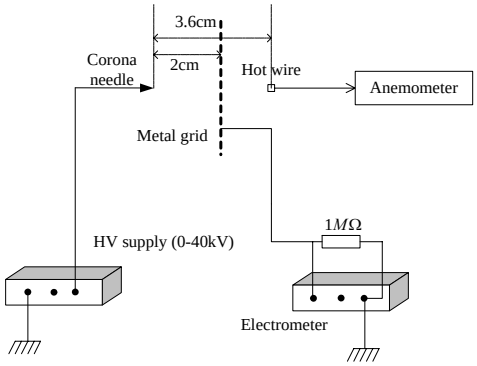

Fig. 2 Experiment set up for the EHD flow measurements

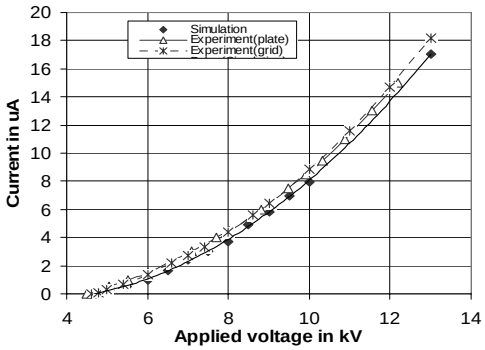

Fig. 3. Calculated and experimental I-V characteristics for metal grid and plate as a cathode.

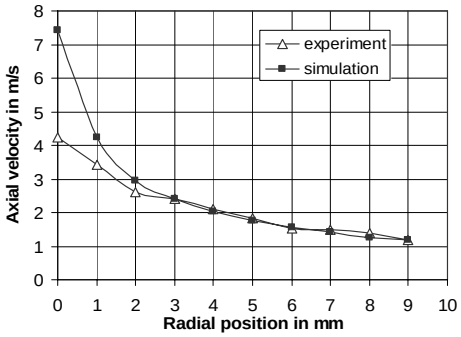

Fig. 4. Numerically calculated and experimental axial velocity profiles 3.6 cm away from the tip of 95 μm needle 2cm above the grounded metal grid at 13 kV.

The axial flow velocity was measured along the points in the radial direction and the results are shown in Figure 4. Agreement between numerical predictions and experimental data is very good, but only for the radial coordinates larger than 2 mm. At points on the symmetry axis the difference is much larger and it is suspected that the laminar flow model is not adequate in this situation: a very fast and concentrated air jet would need a turbulent model for better accuracy. A finite probe size (in the order of 5 mm) can be also blamed for the lack of a closer agreement.

B. EHD Flow Dynamics

The above-presented investigations were done based on the assumption that both the electric and the gas flow fields are in their steady state. Our next research interest is to investigate how the EHD flow develops to its full pattern, how long it takes to grow to the steady state and which factors affect the process dynamics.

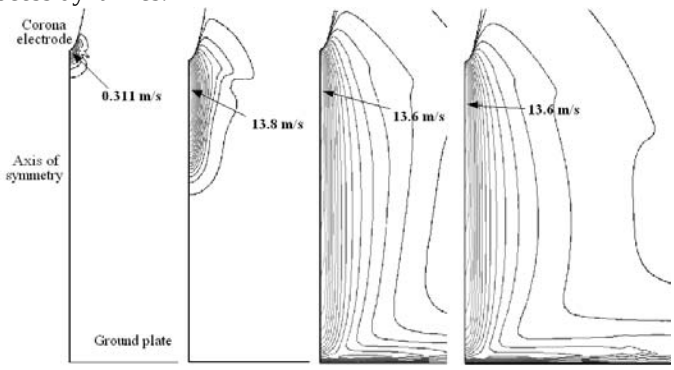

(a) 0.1us (b) 0.5ms (c) 5.0ms (d) steady-state

Fig. 5 Velocity contours at 10 kV and different instants of time

Based on the well accepted assumption that the drift velocity of ions is usually about two orders of magnitude larger than the typical velocity of the gas flow [5], it may be safe to say that the electric field reaches its steady state much earlier than the gas flow field. “The typical propagation time of the ionizing front (breakdown streamer in a corona discharge) in a similar system is 50ns [12]”. Therefore, in order to simplify the analysis, we assumed that the electric field has already been in its steady state when the gas flow begins to develop. The dynamic models for the corona discharge are available [13], but this should not affect the results for the gas flow dynamics. The development of the secondary EHD flow is a surprisingly fast phenomenon. The EHD flow dynamics has been simulated in the pin-plate configuration. The governing equations are similar to those for the steady state except for the velocity time derivative. A fixed time step of 1μs or 10μs has been set. At each instant of time the solution for the air flow has to converge before continuing to the next time step [14].

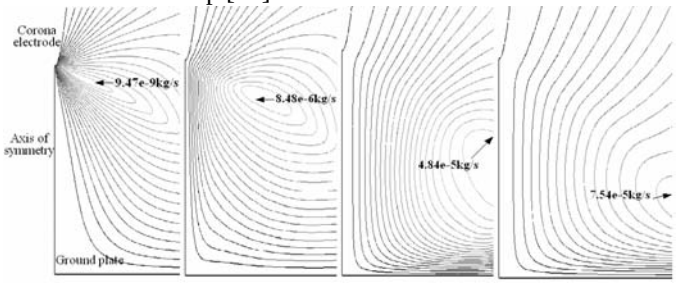

(a) 1.0 μs (b) 1.0 ms (c) 10 ms (d) steady state

Fig. 6 Velocity streamlines (mass flow contours) at different instants of time at 10 kV

Figures 5 and 6 show the airflow velocity magnitude contours and the velocity streamlines at some instants of time when the applied voltage is equal to 10 kV. The maximum values are indicated in the figures with 20 contour lines between the maximum value and 0. A localized airflow appears close to the corona electrode tip a few microseconds after applying the high voltage (Figures 5 (a) and 6 (a)). The air jet created by the volume Coulomb force propagates in both axial and radial directions. The maximum velocity increases and so does the maximum mass flow, which can be seen from Figures 5 (b) and 6 (b). In most of the air gap the flow is in the axial direction, but at the ground plate it is diverted into the radial direction (Figures 5 (c) and 6 (c)). During the evolution of the EHD flow, the center of the vortex moves from a location close to the needle tip to the right bottom corner of the calculation domain, as shown in Figure 6, from (a) to (d). A steady-state flow is reached after approximately 0.1s.

C. The Effect of External Gas Flow on Corona Discharge

Under standard atmospheric pressure, the EHD flow has a negligible effect on the corona discharge, because the air velocity is much smaller than the velocity of moving ions [10]. This may not be true when the airflow is produced externally and the velocity can reach much higher values. This problem was investigated in the point-grid system placed in a tube.

The metal plate from the previous configuration had been replaced for this study with a metal wire grid. From the electrical point of view the grid in the corona discharge plays practically the same role as the metal plate, what has been verified experimentally[2]. However, the grid's role in the airflow is quite different from that of the plate, as it allows the air to flow through instead of blocking the air paths and forcing the airflow to change direction to the radial one. The effect of the grid on turbulence onset has also been neglected; we believe that this effect is not significant for the solution in the air gap between the electrodes. Both electrodes were placed coaxially in a cylindrical dielectric container with radius R_c=2cm. An axial flow with different velocities was enforced in both directions. The 2D computational model of the problem in the cylindrical coordinates is shown (Figure 7).

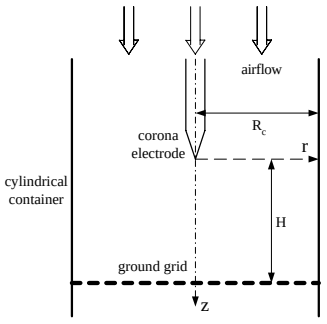

Fig. 7 Computational model for the corona discharge in an external airflow

The numerical simulation was performed first assuming that voltage applied to the corona electrode is 9 kV and the external airflow is blown in the positive axial direction (+z). The current density on the mesh surface for different values of the airflow velocity is shown in Figure 8. It is clear that at the same point on the ground electrode the current density is larger when an external airflow, in the ion drift direction, is present than when airflow is absent. This can be explained by (3) that in addition to the drift current, the convection component appears which contributes to the total current density. It also can be noticed that with airflow, the current density drops to zero at 0.93 centimeter as compared to 1.22 centimeter without airflow. This means the positive external air flow focuses the ion trajectories to the center of the tube. When the airflow changes its direction, for instance to -10 meters per second, the current density on the ground mesh (shown in Figure 8) is smaller than that without airflow, and it drops to zero at 1.46 centimeter. The numerical results predict a small local minimum of the current density distribution on the axis of the system. While this kind of distribution was measured for some gas composition, in the case under investigation it is probably a numerical artifact [6].

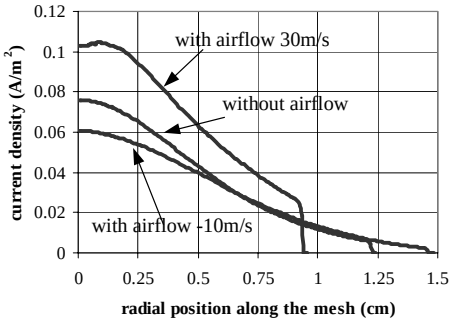

Fig. 8 Current density on the ground mesh for different flow velocities at 9 kV

The airflow also changes the *I-V* characteristics of the discharge; an example for external airflow velocity equal to 30m/s is shown in Figure 9. Although both curves have the same trend, at the same applied voltage the current calculated with the external airflow is larger than that without the airflow. This means that the output electric power increases because of the existence of the external airflow. The power conversion from mechanical to electrical form takes place, and this is what had stimulated research on the electrogasdynamic generators [15] in the past.

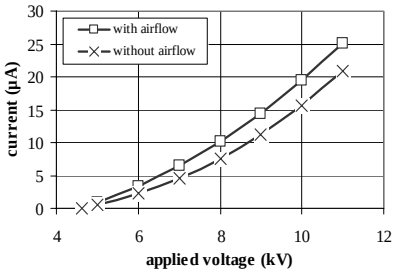

Fig. 9 *I -V* curve with external airflow of 30 m/s and without airflow

Figure 10 presents the relationship between the total corona current and the external airflow velocity: the corona current increases with the increase of the airflow velocity, but becomes smaller when the airflow changes its direction. With the external airflow in the ion drifting direction, the ions are

moved not only by the Coulomb force but also by the airflow. In this process, some mechanical energy is converted into electrical energy. As a result, the current on the ground electrode becomes larger. When the external air flows in the direction opposite to the ion drift, the ions have to overcome the airflow drag on their way to the ground electrode. Some electric energy is consumed in this process and this causes the current decrease.

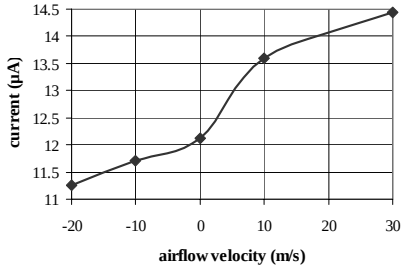

Fig. 10 Corona current versus airflow velocity at V=9 kV

D. EHD Flow in Compressed Gases

When investigating the corona discharge and the EHD flow in compressed gases, the fully coupled model has to be used, since the higher pressures result in lower ion mobility and lower ion drift velocities, which lead to a stronger ion convection effect. The normalized relationship under different operation pressures between the applied voltage and the corona current has been shown in Figure 11. All three curves, calculated at 50 atm pressure and one atm pressure, respectively, have the same trend with the corona current rising above the onset level approximately as a square function of the applied voltage. A noticeable difference between the two curves calculated at 50 atm pressure by using the decoupled and fully coupled models can be observed. The difference between both curves increases with the increase of the applied voltage. This phenomenon confirms that at pressures higher than atmospheric one the effect of EHD flow on corona discharge becomes significant and should be considered, although at atmospheric pressure an opposite conclusion has been drawn [16].

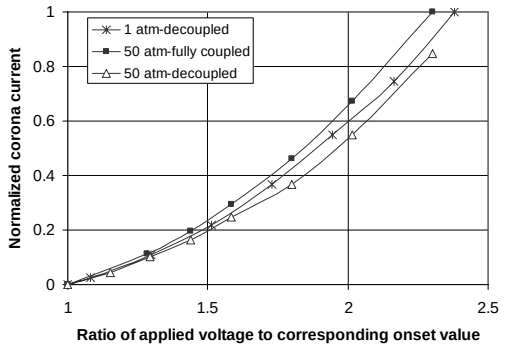

Fig. 11 Normalized corona current versus normalized applied voltage at different pressures with decoupled and fully coupled models.

IV. EHD Flow in Electrostatic Precipitator

The EHD phenomena during the electrostatic precipitation process are extremely complex, mainly due to three fields being present at the same time: gas flow, electrostatic field, and particle dynamics. These three fields are mutually coupled with each other, as shown in Figure 12 [17]. In this study the focus is on the interaction between the electric field and the gas flow interaction: the electrostatic field interferes with the fluid field through the EHD flow, while the gas flow modifies the electric field by ion convection effect. Therefore, the fully coupled model is used.

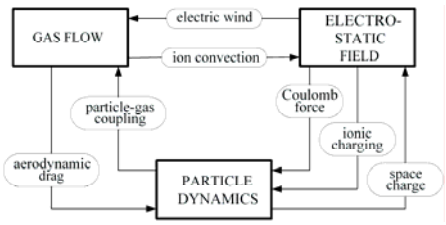

Fig.12 Fields and their interactions during the precipitation process

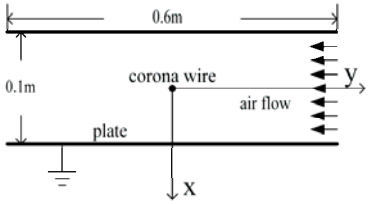

Fig. 13 Two-dimensional computational model of a wire-plate ESP

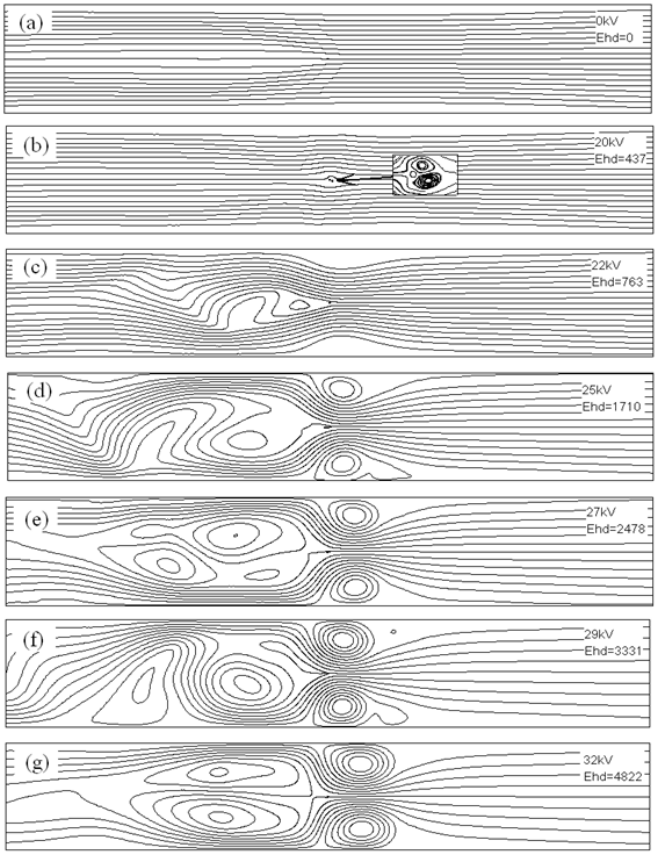

Fig. 14 Streamlines for the gas flow in the precipitator channel for inlet flow velocity equal to 0.2 m/s and varying corona wire voltage

For a wire-plate ESP, a two-dimensional computation model can be considered with the simulation domain of $-0.05<x<0.05$ and $-0.3<y<0.3$ in the Cartesian coordinates, as depicted in

Figure 13. The main gas flows in the negative *y* direction with the velocity between 0 to 2 m/s. The applied voltage varies from 0 to 32 kV. The governing equations are those for the fully coupled corona model and the standard *k-ε* turbulent model for gas flow [18, 19].

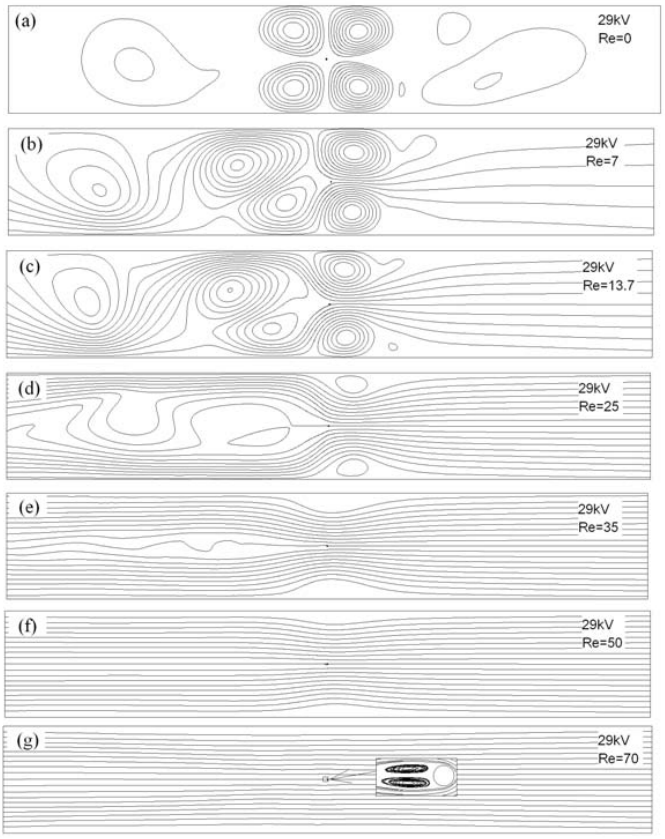

Fig. 15 Streamlines for the gas flow in the precipitator channel for the applied voltage is equal to 29 kV and varying velocity of the main gas flow

At the same inlet gas flow velocity equal to 0.2 m/s, several cases with different applied voltages were calculated to investigate how the secondary EHD flow produced by corona discharge modifies the main gas flow pattern. For these cases, the wire-based Reynolds number is kept constant at 13.7 (the corona wire diameter 1mm and the gas kinematic viscosity 1.46e-5 m^2/s); the *Ehd* number increases with the increase of the applied voltage and the related space charge density on the corona wire. Figure 14 (a to g) displays the streamline patterns for different *Ehd* numbers. When the *Ehd* number is equal to zero (a), no EHD flow exists in the channel and the main gas flow dominates. For relatively small *Ehd* numbers (b), when the applied voltage is slightly above the onset level, the corona discharge is weak and so is the EHD flow: only two tiny vortices appear on the upwind side and very close to the corona wire. When the applied voltage increases further (c), the EHD flow shows small effect on the downwind side: a thin oscillating wake is generated. In the case of (d), the *Ehd* number is larger than 1000. The EHD flow begins to affect the whole flow pattern: there are two large vortices close to the collecting plates and downwind oscillations become wider. In the cases from (e) to (g), the flow continues its evolution with two upwind vortices growing bigger while the downwind oscillations eventually form two larger vortices. In the case shown in (g), four large stable vortices have been fully developed and the effect of the EHD flow is not a near-wire phenomenon anymore. The whole flow pattern has been modified into a totally different one.

Figure 15 (a to g) presents the airflow pattern evolution when the Reynolds number varies and the *Ehd* number is constant. The pattern (a), with four fully developed vortices surrounding the wire, appears without any primary flow and the EHD flow occupies the whole channel. The two large vortices downstream narrow down with the increase of the main flow velocity (patterns b to d). Gradually the primary flow overcomes the EHD flow. At a relatively large Reynolds number equal to 35, pattern (e) presents a narrow wake oscillating downstream and a noticeable waist close to the wire. Finally, when Reynolds number reaches 70 (g), the main gas flow dominates the channel, the average stream lines are parallel to the walls, and von Karman vortices are created behind the corona wire

V. EHD Flow in Electrostatic Propulsion Unit

The electrostatic propulsion device studied in this paper consists of two mechanically connected electrodes: a thin corona wire and a much thicker ground electrode without any sharp points. These two electrodes are parallel with each other to form a triangular structure with spacers made of light wood. When a sufficiently high voltage applied between these two electrodes, electrical corona discharge takes place and the EHD flow is created. The reactive force of the EHD flow driving force makes the propulsion possible [20].The propulsion experiment was carried out using the set up shown in Figure 16.

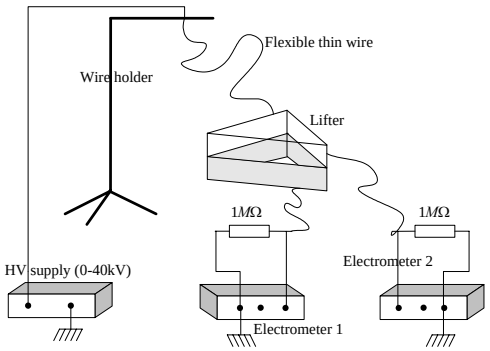

Fig. 16 Set up for the levitation experiment

Figure 17(a) shows the picture taken during one of the stable propulsion experiments.

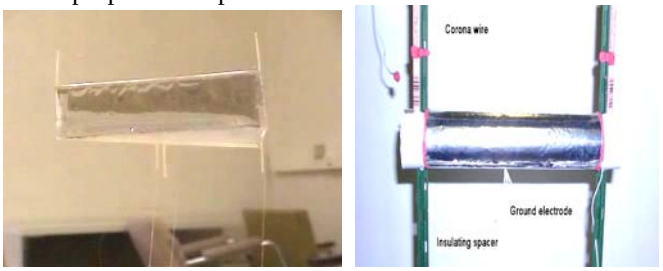

Fig. 17 (a) The lifter during the levitation experiment and (b) lifter used in the force measurement experiment

Figure 18 shows photos taken in the dark during the levitation experiment. The corona glow surrounding the wire

can be seen clearly in Figure 18 (a). It should also be pointed out that the bipolar corona discharge was taking place at some points on the ground electrode. These points were created during fabrication and were evidently located close to the spacer. The negative corona was generated from the corona wire, while the positive one from some sharp points on the ground electrode. Figure 18 (b) shows the moment when the spark was triggered next to those points [21].

(a) (b)

Fig. 18 Photos of (a) stable levitation and (b) spark discharge taken during the levitation experiment in dark

As a result of the corona discharge the ionic species are produced in air and the force *Fe* is generated due to interaction of the electric field between both electrodes and space charge density. The ions on their way to the ground electrode give up their momentum to the neutral air molecules in the process of producing EHD flow. Treating electrodes and the space charge as one system, the net force acting on it is equal to *Fe*, which is the reaction force to the one that drives the airflow. Therefore, the whole system operates like a jet engine with the thrust causing the system levitation [20].

Figure 17 (b) shows the experiment setup for propulsion force measurement. During the experiment the lifter is attached to a light foam base and placed on an accurate electric scale. The reading of the scale is calibrated to a zero value. Then the thrust force produced at different values of the supply voltage is measured as a negative reading on the scale.

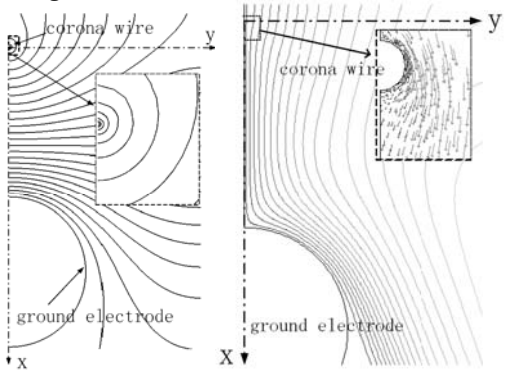

(a) (b)

Fig. 19 (a) Equipotential lines in the levitation device and (b) the airflow pathlines between both electrodes.

The performance of the propulsion unit is simulated with the proposed numerical model to reveal the crucial role of the EHD flow. Figure 19 (a) shows the predicted equipotential lines between the two electrodes. It can be seen that the gradients of the electric potential, located near the origin and at the intersection of the *x* axis and the surface of ground electrode, are much higher than the gradients at the other area; consequently the electric field reaches very high values at these points. Figure 19 (b) presents the airflow pathlines in the whole air gap with details of the air velocity vectors at points close to the corona wire. Driven by the Coulomb force, most of the air flows from the corona wire to the ground electrode in the *x* direction, and then changes to the *y* direction because of the resistance of the ground electrode.

Figure 20 shows the experimental and the simulated *I-V* characteristics of the levitation unit. These two curves have slightly different onset voltages, 7.5 kV from the experiment and 8.8 kV for the simulation, which is probably caused by the fact the surface of the wire and the ground electrode is assumed to be ideally smooth in the simulation model. Some sharp points, impossible to avoid during the device fabrication, can trigger the corona discharge at a lower voltage level. The two curves have almost the same slope from onset voltage to around 20 kV with the experimental one being lower, and then the experimental results become steeper and cross the simulation curve at 23 kV. The spark discharge in the experiment is observed at 25.8 kV. It is believed that the bipolar corona discharge from the ground electrode contributes to the sudden increase in the experimental curve. At lower voltage levels, air partial breakdown takes place in the vicinity of the thin corona wire, and only the negative corona discharge occurs. When the supplied voltage reaches a certain level, the sharp points on the ground electrode surface begin to contribute a significant component of positive corona resulting in the sudden increase of the corona current

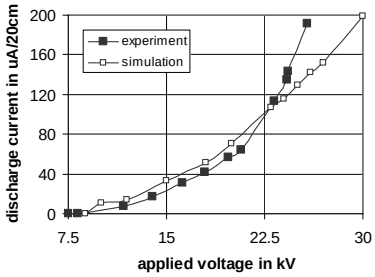

Fig. 20 Comparison of experimental and calculated *I-V* characteristics

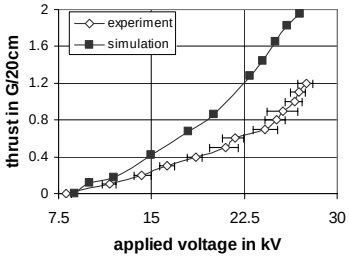

Fig. 21 Thrust versus applied voltage characteristics

Figure 21 displays experimental and numerical characteristics of the thrust versus applied voltage. For the same applied voltage, the measured thrust is smaller than the calculated one. This is consistent with what is shown in Figure 20 since a smaller current results in a smaller thrust. However, if the voltage is larger than 22.5 kV, a larger experimental current results in a smaller thrust. While it seems to be surprising at the first look, this is consistent with the previous suspicion that the bipolar corona discharge takes place when the applied voltage reaches a value of about 22.5 kV. The

positive corona discharge contributes to the current increase but causes the decrease of the thrust, since the positive space charge neutralizes the negative one. Thus the reduced space charge density results in decreased Coulomb force, and the thrust.

VI. Conclusions

The numerical simulation, experimental studies and the potential applications of the EHD flow produced by electrical corona discharge were presented in this paper. A comprehensive numerical model (decoupled and fully coupled) of the EHD flow produced by electrical corona discharge has been introduced. The reliability of the proposed model has been verified with a series of experimental measurements. The characteristics of the EHD phenomena with different system configurations, with or without external gas flow and under different operational pressures have been revealed. The important roles of the EHD flow in the ESPs and the electrostatic propulsion unit were investigated. The following conclusions can be drawn:

1) The decoupled model for corona discharge simulation in air is valid for systems without external gas flow and under standard atmospheric. Otherwise, the fully coupled corona model should be employed.
2) An external airflow alters the ionic charge transport through the ion convection effect and further distorts the characteristics of the corona discharge. The intensity of this effect depends on the airflow velocity magnitude and directions.
3) The dynamic evolution of the EHD flow depends on not only the air gap geometry but also the applied voltage. Usually it takes several milliseconds to reach the steady state. The higher the applied voltage, the shorter the time takes to reach the steady EHD airflow.
4) A higher gas pressure results in lower ion mobility and drift velocity. The ion convection effect increases with an increase in the gas pressure. This means that at high pressures the ion convection current plays an important role in formation of the corona current and that the corona current is no longer proportional to the ion mobility.
5) A higher pressure not only compresses the gas and changes its properties, but also narrows the drift region through which the ionic charges travel from the corona electrode to the ground electrode.
6) The presence of secondary EHD flow in the precipitation channel of ESP modifies the gas flow and makes the entire flow pattern very complex. The level of modification depends on the corona electric field and the gas flow parameters.
7) The idea of electrostatic propulsion has been proved experimentally. The levitation device was able to produce enough thrust to lift its own weight plus a small load if enough voltage was supplied between its two electrodes.

References

[1] L. Zhao, "Electrohydrodynamic flow in air produced by electric corona discharge-numerical and experimental studies of the EHD phenomena in the electrostatic levitation unit and the industrial electrostatic precipitators," Ph.D. dissertation, Dept. Elect. And Computer Eng., University of Western Ontario, London, ON, CANADA, 2006.

[2] L. Zhao and K. Adamiak, "EHD flow in air produced by electrical corona discharge in pin-plate configuration," *J. of Electrostat.*, vol. 63, pp.337-350, 2005.

[3] B. Eliasson and U. Kogelschatz, "Basic data for modelling of electrical discharges in gases: oxygen," Bown Boveri, June 1986 unpublished technical report.

[4] J.S. Chang, A.J. Kelly and J.M. Crowley, *Handbook of Electrostatic Processes*, Marcel Dekker, Inc., New York, 1995

[5] T. Yamamoto and H.R. Velkoff, "Electrohydrodynamics in an electrostatic precipitator", *J. of Fluid Mech.*, vol.108, pp. 1-18, 1981.

[6] K. Adamiak and P. Atten, "Simulation of corona discharge in point-plane configuration", *J. of Electrostat.*, vol.61, pp.85-98, 2004.

[7] K. Adamiak, J. Zhang and L. Zhao, "Finite element versus hybrid BEM-FEM techniques for the electric corona simulation", *The Electrotechn. Rev.*, No. 10, pp. 753-756., 2003.

[8] A.M. Meroth, T. Gerber, C.D. Munz, P.L. Levin and A.J. Schwab, "Numerical solution of nonstationary charge coupled problems", *J. of Electrostat.*, vol. 45, pp.177-198, 1999.

[9] *FLUENT 6.2 User's Guide*, Fluent Inc.

[10] L. Zhao and K. Adamiak, "Effects of EHD and external airflows on electric corona discharge in pin-plate/mesh configuration," *IEEE Trans. on Ind. Appl.*, vol.45, pp. 16-21, January-February 2009.

[11] L. Zhao and K. Adamiak, "Numerical simulation of corona discharge with the effect of EHD flow in compressed gases," in *Proc. of 2008 Annal. Meeting of the Electrostatics Society of America*, Minneapolis, MN, USA, June 17-19, 2008, paper C2.

[12] J. Batina, F. Noël, S. Lachaud, R. Peyrous and J.F. Loiseau, "Hydrodynamical simulation of the electric wind in a cylindrical vessel with positive point-to-plane device," *J. of Phys., D: Appl. Phys.*, vol. 34, pp.1510-1524, 2001.

[13] J. Zhang and K. Adamiak, "A multi-species DC stationary model for negative corona discharge in oxygen; point-plane configuration," in *Proc. of 2005 Electrostatics Society of America Annual Meeting*, Edmonton, Canada, June, 2005, pp. 153-164.

[14] L. Zhao and K. Adamiak, "Dynamics of EHD flow in pin-plate configuration generated by electric corona discharge in air," In *Recent Developments in Applied Electrostatics,* K. Sun and G. Yu, Eds., Elsevier, 2004, pp. 29-32.

[15] M.J. Mulcahy and W.R. Bell, "Electrostatic Generators," in *Electrostatics and Its Applications*, A.D. Moore, Ed, J. Wiley and Sons, New York 1973, pp. 148-179.

[16] L. Zhao and K. Adamiak, "Effects of EHD and external air flows on electric corona discharge in pin-plate configuration," in *Proc. of the IEEE-IAS 2005 Annual Meeting*, Hong Kong, October, 2005, vol. 4, pp. 2584-2589.

[17] G.A. Kallio and D.E. Stock, "Flow visualization inside a wire-plate electrostatic precipitator," *IEEE Trans. on Ind. Appl.*, vol. 26, pp. 503-514, 1990.

[18] L. Zhao, E. dela Cruz, K. Adamiak, A.A. Berezin and J.S. Chang, "A numerical model of a wire-plate electrostatic precipitator under electrohydrodynamic flow conditions," in *Proc. of 10th Int. Conf. on Electrostatic Precipitation ICESP X*, Cairns, Australia, June 25-29, 2006, paper 7B3.

[19] L. Zhao and K. Adamiak, "Numerical simulation of the electrohydrodynamic flow in a single wire-plate electrostatic precipitator," *IEEE Trans. on Ind. Appl.*, vol. 44, pp 683-691, 2008.

[20] L. Zhao and K. Adamiak, "Numerical analysis of forces in an electrostatic levitation unit," *J. of Electrostat*., vol. 63, pp.729-734, 2005.

[21] L. Zhao, K. Adamiak, P. Leonard and G.S.P. Castle, "Electrostatic levitation unit: experimental measurements versus numerical simulation," in *Proc. of 2005 Electrostatics Society of America Annual Meeting*, Edmonton, Alberta, June 2005, pp.201-213.